

NON-HYDROSTATIC MODELING OF COASTAL LEVEE OVERFLOWS

Takenori Shimozone¹, Hiroki Ikezawa¹ and Shinji Sato¹

Abstract

The spatial resolution of coastal flood simulations has improved with enhanced computational power and increasing availability of high-resolution topographic data. However, grid refinement does not necessarily enhance the accuracy of standard flood models based on nonlinear shallow water equations (NSWE), because flows over locally steep topographies may be significantly affected by non-hydrostatic pressure induced by vertical flow acceleration. In this paper, we present a depth-integrated, non-hydrostatic model for simulating flows over steep landforms such as coastal levees. The model is constructed from fully nonlinear Boussinesq-type equations with a modification term to suppress oscillatory behaviors in overflow solutions. The proposed model accurately simulates the experimental data for steady overflows, whereas the NSWE model significantly underestimates the overflow rate in cases of large overflow depths.

Key words: overflow, coastal levee, Boussinesq-type equation, non-hydrostatic pressure

1. Introduction

Over the past few decades, the coastal flood model has developed into an essential tool for mitigating coastal disasters such as tsunamis and storm surges. The resolution of the coastal flood model has improved with expanding computational power, providing detailed information of potential flood impacts on coastal communities. Airborne LiDAR technology has also advanced, providing us with meter- or even sub-meter-scale digital elevation models (DEMs). Therefore, the model resolution is expected to further improve in future decades. However, the increasing grid resolution reveals finer-scale topographic features, which can be man-made structures (such as coastal levees and seawalls) or natural landforms (coastal dunes and hills). Over steep landforms, the vertical flow acceleration might violate the hydrostatic assumption in the typical flood models. Under this condition, grid enhancement will not improve the model accuracy beyond a certain limit, unless the hydrostatic assumption is relaxed. To demonstrate this scenario, we conducted a case study of coastal flooding over a levee-protected area during the 2011 Tohoku tsunami (Shimozone and Sato, 2016).

If the non-hydrostatic pressure is incorporated in the model equation, the model performance will respond to the grid refinement. Some researchers have relaxed the topographical restrictions by correcting the nonlinear shallow water equation. In an early attempt, Dressler (1978) derived the shallow water equation in orthogonal curvilinear coordinates fitted to the bottom surface, thus accounting for the flow curvature effect. The curvilinear approach was also adopted in later modifications of the shallow water equations (Bouchut et al., 2003 and Keller, 2003). More recently, Dutykh and Clamond (2011) derived a variant of the equations through the variational principle. Fenton (1996) pointed out drawbacks of the curvilinear approach and added a centrifugal term to the shallow water equations for steady flows. Although these modified shallow water equations incorporate the bed slope effect, their performances were confirmed only in very simple problems; hence, their applicability to flood simulations is not known.

Alternatively, we could apply the higher-order extensions of the shallow water equations in terms of the shallowness parameter (the relative depth to wave length) known as the Boussinesq-type equations. As the shallowness parameter and bed slope are implicitly assumed to be of the same order, this class of equations can account for the effects of steep bed slopes. The Boussinesq-type equations accurately simulate the propagation of relatively short waves in coastal water, but have rarely been applied to flood simulations

¹ Dept. of Civil Engineering, The University of Tokyo, Hongo 7-3-1, Bunkyo-ku, Tokyo, 113-8656, Japan.
shimozone@coastal.t.u-tokyo.ac.jp

over complex coastal topography, possibly because the higher-order terms (called dispersion terms or Boussinesq terms) remove the hyperbolic property of the equations, and lead to oscillatory behaviors in solutions. Consequently, in flood simulations involving transient flows and dry/wet interfaces, the Boussinesq-type models should be improved for higher model robustness. There have been some attempts to develop shock-capturing Boussinesq-type models for wave overtopping simulations (Lynett et al., 2010; Tonelli and Petti, 2013), but their focus was to improve wave propagation prior to overtopping by incorporating frequency dispersion capabilities. The role of the Boussinesq terms in flood flows over steep landforms is not well understood.

The present study is aimed at exploring the effect of the non-hydrostatic pressure in coastal levee overflows caused by tsunamis or storm surges. For this purpose, we develop a depth-integrated, non-hydrostatic model based on fully nonlinear Boussinesq-type equations. To control the excessive oscillations in solutions, we follow the approach of Madsen et al. (1991), and modify the original equation by introducing a free parameter. The model is validated in comparisons with experimental results for steady flows over trapezoidal levees. To clarify the non-hydrostatic pressure effect on overflow characteristics, we compare the model results with those of the nonlinear shallow water equations.

2. Model Description

2.1. Governing equations

Boussinesq-type equations differ by their variable types and truncation orders. For transient water flows (see Figure 1), the model equation should be datum-invariant. Here we employ the fully nonlinear weakly dispersive wave equations independently derived by Goto (1984) and Seabra-Santos et al. (1987), which are expressed as

$$d_t + Q_x = 0, \quad (1)$$

$$Q_t + \left(\frac{Q^2}{d} \right)_x + gd\eta_x = \left(\frac{d^3}{3} \Gamma_1 - \frac{d^2}{2} \Gamma_2 \right)_x + b_x \left(\frac{d^2}{2} \Gamma_1 - d\Gamma_2 \right) \quad (2)$$

with

$$\Gamma_1 = u_{ttx} + uu_{xx} - u_x^2, \quad (3)$$

$$\Gamma_2 = b_x(u_t + uu_x) + u^2 b_{xx}, \quad (4)$$

where t is time, x is the horizontal coordinate, and the subscript x or t denotes a derivative with respect to x or t , respectively. g is the gravitational acceleration, d is the total water depth, u is the depth-averaged horizontal velocity, and Q is the flow rate per unit width ($= du$). η and b also denote the elevations of the water surface and bed, respectively. To derive these equations, we integrate the 2D continuity and Euler's equations over the depth and retain terms up to second-order of the shallowness parameter and the bed slope. The RHS of Equation (2) contains higher-order terms, which are ignored in the nonlinear shallow water equations.

The vertical distribution of pressure corresponding to the above equations is given by

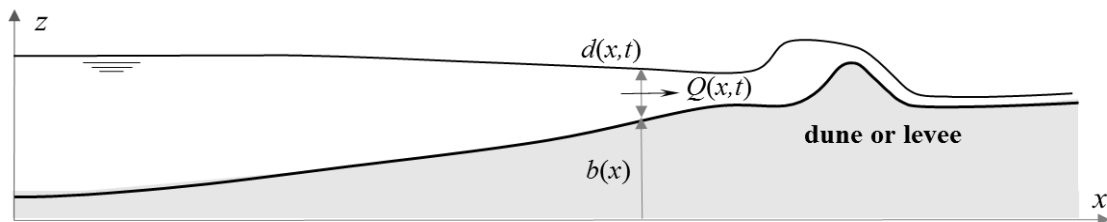


Figure 1. Definitions of axes and flow variables.

$$p = \rho g (\eta - z) + \rho \left[\left\{ \frac{(z-b)^2}{2} - \frac{d^2}{2} \right\} \Gamma_1 - (z-\eta) \Gamma_2 \right], \quad (5)$$

where p is pressure, z is the vertical coordinate and ρ is the density of water. The second term on the RHS of Equation (5) represents the non-hydrostatic pressure due to vertical flow acceleration, which quadratically varies in the vertical direction. This formulation accounts for the centrifugal effect in the transient flows over coastal levees. However, these equations yield excessive oscillations over the levee crest in the overflow simulations, which may lead to model instability.

Similarly to Madsen et al. (1991), we improve the Boussinesq-type equations in this regard by adding a modification term to Equation (2) as:

$$\Gamma_3 = \alpha d^3 (u_t + uu_x + g\eta_x)_{xx}, \quad (6)$$

where α is a small parameter. This modification term can be shown to be fourth-order in the shallowness parameter; therefore, adding it to Equation (2) does not affect the order of magnitude of the equation. As is well known, the linear dispersion relation in wave simulations is optimized at $\alpha = 1/15$. As described later, we use the degree of freedom to control the oscillatory behaviors in overflow solutions. In addition, we insert a frictional term based on the Manning formulation to simulate the bed friction. The resulting momentum equation reads

$$Q_t + \left(\frac{Q^2}{d} \right) + gd\eta_x = \left(\frac{d^3}{3} \Gamma_1 - \frac{d^2}{2} \Gamma_2 \right) + b_x \left(\frac{d^2}{2} \Gamma_1 - d\Gamma_2 \right) + \Gamma_3 - \frac{gn^2}{d^{7/3}} Q|Q|, \quad (7)$$

where n is the Manning roughness. Equations (1) and (7) form the model equations in our present study.

To investigate the properties of the model equations in flow simulations, we consider steady flows over a uniform slope s . As evident from Equation (1), the flow rate Q becomes horizontally uniform, and Equation (7) reduces to an equation in a single variable d . To simplify the expression, we neglect the bed friction, which exerts a relatively small effect over steep bed slopes. The resulting single variable-equation becomes

$$d^2 \{ 3\alpha gd^3 - (3\alpha + 1)Q^2 \} d_{xxx} - Q^2 (36\alpha + 1) d_x^3 + (27\alpha + 2) Q^2 d d_x d_{xx} + 3 \{ Q^2 (1 + s^2) - gd^3 \} d_x - 3gd^3 s = 0. \quad (8)$$

The first three terms on the LHS of Equation (8) describe the non-hydrostatic pressure effect. The balance among these three terms is tuned by the modification parameter α . As this third-order nonlinear differential equation is difficult to solve, we linearize it by expressing d as a uniform water depth h plus a small deviation $\zeta(x)$ following Fenton (1996); namely, we set $d = h + \zeta$. Neglecting the higher-order terms in ζ , we have

$$h^2 \left\{ \alpha - \left(\alpha + \frac{1}{3} \right) F_r^2 \right\} \zeta_{xxx} + \{ F_r^2 (1 + s^2) - 1 \} \zeta_x - 3 \frac{s}{h} \zeta - s = 0, \quad (9)$$

where F_r is the Froude number ($= Q/h\sqrt{gh}$). Equation (9) is a third-order linear differential equations in ζ . We seek solutions of the form $\zeta = e^{\lambda x}$. To this end, we find the characteristic equation for the homogeneous problem:

$$\left\{ \alpha - \left(\alpha + \frac{1}{3} \right) F_r^2 \right\} h^2 \lambda^3 + \{ F_r^2 (s^2 + 1) - 1 \} \lambda - \frac{3s}{h} = 0 \quad (10)$$

The discriminant of the cubic equation is given by

$$\Delta = 4(1 - F_r^2)^3 \left\{ \alpha - \left(\alpha + \frac{1}{3} \right) F_r^2 \right\} + O(s^2), \quad (11)$$

where the square terms of the bed slope are neglected to truncate the discriminant (the exact discriminant is very lengthy). From this discriminant, we deduce the forms of the solutions. When $F_r > 1$ (supercritical flow) or $F_r < \sqrt{3\alpha/(3\alpha + 1)}$ (sub-critical flow), Δ is positive; thus, the characteristic equation has three real roots, and the water surface variation is described by a combination of exponential functions. When $\sqrt{3\alpha/(3\alpha + 1)} < F_r < 1$ (subcritical flow), the characteristic equation has one real and two imaginary roots, so the water surface exhibits oscillatory behaviors. The parameter α modifies the range of F_r wherein undulations appear in the water surface.

The modified momentum equation correctly describes the free overflow processes, wherein which the flow suddenly changes from subcritical to supercritical on the crests of convex landforms. The modification term exerts no significant effect on supercritical flows ($F_r > 1$), but changes the wavelength of the undulation in subcritical flows ($F_r < 1$). According to Equation (11), the undulations can form immediately upstream of the critical depth on the crest. The original equation ($\alpha = 0$) affords oscillatory solutions in all subcritical flow regions, whereas the modified equation with small positive α admits oscillatory solutions only for F_r below the trans-critical condition ($F_r = 1$). For example, if we set $\alpha = 1/15$, the undulations appear within the range $0.41 < F_r < 1$. In Section 3, we will choose this parameter by comparing the model results with experimental data.

2.2. Numerical method

The numerical method is similar to that of Shimozono et al. (2015). We hybridize a high-order finite difference scheme, hereafter called the base scheme, with a shock capturing scheme based on Yee et al. (1999). First, the model equations are solved in the base scheme (the homogenous part of the equations). To the base solution, we add the nonlinear dissipation associated with the shock-capturing scheme. The applicability of the shock-capturing model to levee overflows was confirmed in simulations of nonlinear shallow water equations (Hu et al., 2000; Tuan and Oumeraci, 2010; Lynett et al., 2010; Tonelli and Petti, 2013). By virtue of its conservative properties, the hydrostatic model converges to weak solutions by the momentum principle or the Bernoulli equation, depending on the flow type (Stelling and Duinmeijer, 2003). Variants of this model have been employed in two-dimensional simulations of coastal flooding in actual areas protected by levees (Le Roy et al., 2014; Shimozono and Sato, 2016). More recently, researchers have simulated nearshore wave processes (including wave breaking) by applying the shock capturing scheme to the Boussinesq-type equations (Bonneton et al., 2011; Roeber et al., 2010). The present model is regarded as a variant of these models.

To simplify the model representation, we compactly rewrite Equations (1) and (7) as

$$U_t + F_x = S \quad (12)$$

where U , F , and S are vectors given by

$$U = \begin{bmatrix} d \\ Q \end{bmatrix}, \quad F = \begin{bmatrix} Q \\ Q^2/d + gd^2/2 \end{bmatrix}, \quad S = \begin{bmatrix} 0 \\ -gdb_x - \frac{gn^2}{d^{7/3}} Q|Q| + G \end{bmatrix} \quad (13)$$

with

$$G = \left(\frac{d^3}{3} \Gamma_1 - \frac{d^2}{2} \Gamma_2 \right)_x + b_x \left(\frac{d^2}{2} \Gamma_1 - d\Gamma_2 \right) + \Gamma_3. \quad (14)$$

First, Equation (12) is discretized by the finite difference method on a regular grid. The base scheme is a high-order finite difference scheme for dispersive equations, proposed by Wei and Kirby (1995). The Adams–Bashforth–Moulton method is used for the time integration, whereas the spatial discretization is performed by fourth-order operators for the non-Boussinesq terms and by second-order finite differences for the Boussinesq terms.

The characteristics-based dissipation term is based on the homogeneous part of Equation (12) and applied at the end of the predictor-corrector step. Setting U^* as the numerical solution of the base scheme, the solution in the next time step is calculated by the following conservative form of the finite difference equation:

$$U_i^{n+1} = U_i^{*n+1} + \frac{\Delta t}{\Delta x} (F_{i+1/2}^* - F_{i-1/2}^*), \quad (15)$$

where Δt and Δx are the time step and the grid spacing in the x -direction, respectively, U_i^n is the discrete approximation of U at $x = i\Delta x$ and $t = n\Delta t$, and $F_{i+1/2}^*$ is the dissipative numerical flux defined at the cell center. The second term on the RHS of Equation (15) is a generic term describing the nonlinear dissipation in different shock-capturing methods. The form of $F_{i+1/2}^*$ depends on the utilized type of shock-capturing method. In the Roe–Sweby TVD scheme (Yee, 1989), the dissipative numerical flux is written as

$$F_{i+1/2}^* = \frac{1}{2} P_{i+1/2} \Phi_{i+1/2}. \quad (16)$$

Here $P_{i+1/2}$ is the right eigenvector matrix of the Jacobian matrix dF/dU evaluated by an approximate Riemann solver proposed by Roe (1981). The m th element of the vector $\Phi_{i+1/2}$, denoted by $\phi_{i+1/2}^m$, is written as

$$\phi_{i+1/2}^m = - \left\{ \left| a_{i+1/2}^m \right| - \delta(r_{i+1/2}^m) \left[\psi(a_{i+1/2}^m) - \frac{\Delta t}{\Delta x} (a_{i+1/2}^m)^2 \right] \right\} \beta_{i+1/2}^m, \quad (17)$$

where $a_{i+1/2}^m$ with $m=1, 2$ are the characteristic speeds, which are the eigenvalues of dF/dU , and $\beta_{i+1/2}^m$ is the m th element of the characteristic variables obtained by $P_{i+1/2}^{-1}(U_{j+1}^n - U_j^n)$. The function ψ is introduced to avoid entropy-violating solutions (Harten and Hyman, 1983), while the function δ is the flux limiter function of the smoothness indicator $r_{i+1/2}^m$, defined by

$$r_{i+1/2}^m = \frac{\beta_{i+1+\sigma}^m - \beta_{i+\sigma}^m}{\beta_{i+1}^m - \beta_i^m}, \quad \sigma = \text{sgn}(a_{i+1/2}^m), \quad (18)$$

which prevents the generation of spurious oscillations in the numerical solutions. If the flux limiter lies within the admissible limiter region (Sweby, 1984), the numerical solution corresponds to that of the second-order TVD scheme. Moreover, when $\delta = 0$, the numerical scheme reduces to the Roe-type upwind scheme. To observe the nature of the model equations, we selected a second-order TVD limiter known as the minmod limiter (Roe, 1986).

3. Steady Overflow Simulations

3.1. Steady flows over levees

To investigate the model performance in steady overflow problems, we compared the model results with the experimental data of free overflows on a levee. Simple laboratory tests were conducted in an experimental flume of width 0.9 m. The levee was modeled from smooth material (acrylic material). The cross-section of the levee was trapezoidal (slope = 1/2 at both sides), with a height h_e and crest width L_w of 12 cm and 6 cm, respectively (see Figure 2). The water surface profiles around the levee were measured under different rates of steady flows. The water surface measurements were performed by an image-based technique. The water in the flume was colored with blue dye, and the steady flows around the levee were photographed through the side glass of the flume. To detect the water surface in the images, the water body was separated from the background image. The continuous water surface profiles around the levee were acquired after geometric corrections.

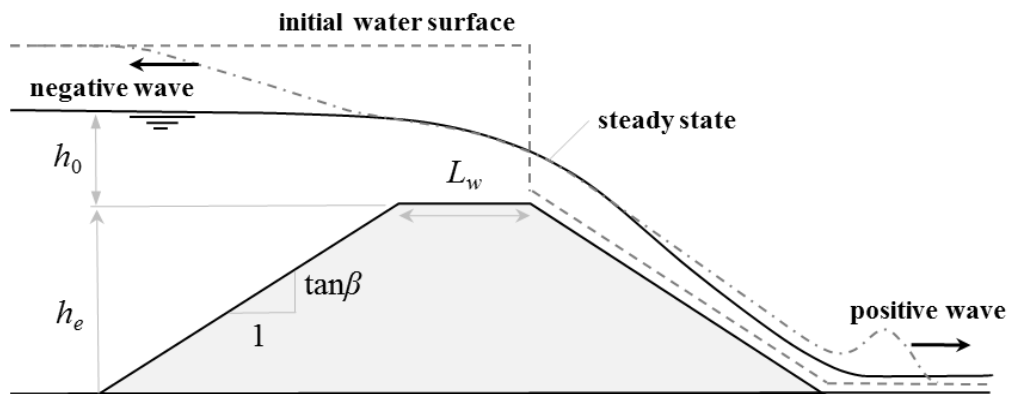


Figure 2. Schematic of steady flows over levees with trapezoidal cross-sections.

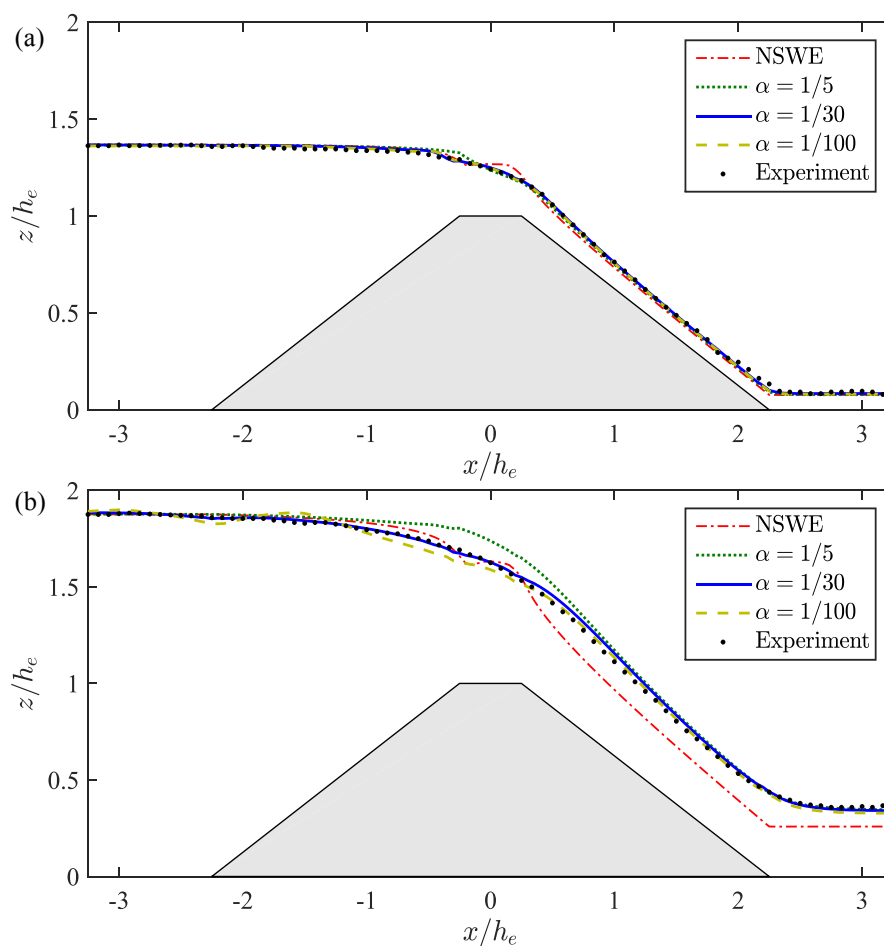


Figure 3. Comparisons of measured and computed water surface profiles around the trapezoidal levee;
 (a) $h_0/h_e = 0.36$. (b) $h_0/h_e = 0.88$.

Numerical simulations were implemented by the time-dependent model in 2.2, although the steady problem is concerned. Solving the steady-state equation for the trans-critical flows is difficult because the boundary conditions on both sides of the levee cannot be known a priori; both the upstream and downstream flows are determined from the levee side. Therefore, using the time-dependent model, we initiate the simulations from the stationary water at constant elevation upstream of the levee crest (indicated by the dashed line in Figure 2). Subsequently, a positive and negative wave propagate in the downstream and upstream directions (indicated by the dash-dot line in Figure 2). Provided that the horizontal beds on both sides are sufficiently long, a steady overflow state develops around the levee. The flow rate of the steady solution can be varied by changing the initial water elevation. The computations were carried out on a grid resolved to $\Delta x/h_e = 0.1$, and terminated when the water surface evolved by less than a specified threshold during one time step. The Manning roughness was set to $n = 0.01 \text{ m}^{-1/3} \text{ s}$. The initial water level was set such that the upstream water level at steady-state matched the experimental water level.

Figure 3 compares the computed and measured water surface profiles around the levee for two overflow depths ($h_0 = 4.3$ and 10.6 cm). Shown are the numerical results of the modified equation with three values of α ($= 1/100, 1/30,$ and $1/5$), and those of the nonlinear shallow water equation (denoted by NSWE). To limit the generation of the subcritical oscillation upstream of the levee, the modification parameter was constrained to small positive values. At the small overflow depth ($h_0 = 4.3$ cm), the results of the four model equations were very similar, except on the levee crest. As the centrifugal effect is small, the higher-order terms exert a minor influence. However, at the higher overflow depth ($h_0 = 10.6$ cm), the non-hydrostatic pressure significantly affects the overflow characteristics. Downstream of the levee, the water surface profile calculated by the NSWE model lies below the experimental profile, indicating that

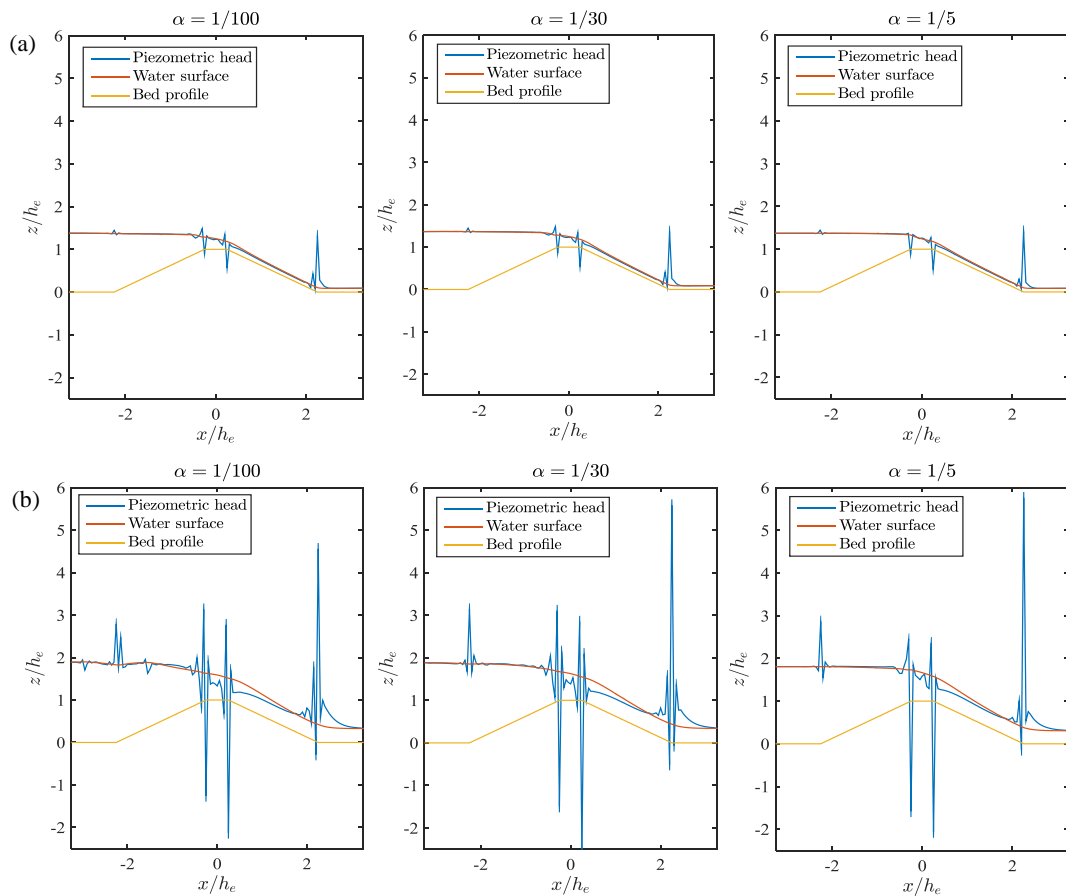


Figure 4. Computed profiles of the piezometric head and water surface around the trapezoidal levee for $\alpha=1/100, 1/30$ and $1/5$; (a) $h_0/h_e = 0.36$. (b) $h_0/h_e = 0.88$.

this model underestimates the overflow rate. The modified equation with $\alpha = 1/30$ yields the best match to the experimental result. The modified equation with $\alpha = 1/100$ generates a slight undulation upstream of the crest, which was not observed in experiments. As α goes to zero, this undulation intensifies to destabilize the computation. Conversely, the modified equation with $\alpha = 1/5$ significantly overestimates the flow depth on the crest. As the α value increases, the convergence to steady-state accelerates because the subcritical oscillation is suppressed.

Figure 4 compares computed profiles of piezometric head from Equation (5) and water surface for $\alpha = 1/100, 1/30$ and $1/5$. The pressure is hydrostatic where the piezometric head profile agrees with the water surface profile. Their discrepancy indicates the generation of the non-hydrostatic pressure due to the centrifugal effect. The results suggest that the non-hydrostatic pressure, which localizes at levee corners, rapidly increases with the overflow depth, since the centrifugal force is proportional to the flow velocity squared. The piezometric head profiles qualitatively agree with measured data from past levee-overflow experiments (e.g. Kato et al., 2012). The profile of large α exhibits weaker fluctuations suggesting that the modification term plays a role of stabilizing the computation.

3.2. Overflow rate

To validate the model over a wider range of flow conditions and levee geometries, we compared the model results with previously published experimental data. For free overflows, Fritz and Hager (1998) proposed an empirical fitting formula to their own and existing data:

$$Q^* = 0.43 + 0.06 \sin[\pi(\zeta - 0.55)], \quad \zeta = \frac{H_0}{H_0 + L_w}, \quad (19)$$

where $Q^* = Q/H_0\sqrt{gH_0}$ is the non-dimensional overflow rate per unit width (the discharge coefficient) and H_0 is the energy head upstream of the levee. Equation (19) expresses Q^* as a function of H_0 and L_w . The various overflow data for levees with 1/2-sloped sides collapse onto the empirical curve in the range $0.1 < \zeta < 0.8$. To compare the model and empirical results, we varied ζ from 0.1 to 0.8 (23 cases), and ran the model for different combinations of L_w/h_e and h_0/h_e ($0.3 < L_w/h_e < 2.0$ and $0.2 < h_0/h_e < 1.1$). The energy head, evaluated as $H_0 = h_0 + 5Q^2/6g(h_0 + h_e)$, is consistent with the formulation of Fritz and Hager (1998), with h_0 evaluated at h_e apart from the upstream toe of the levee. To see the effect of the modification term,

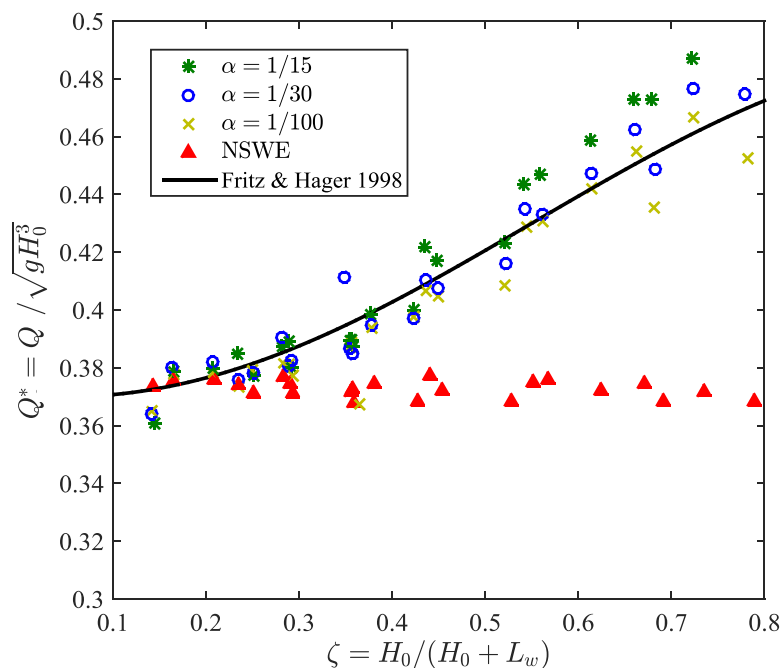


Figure 5. Relationship between Q^* and ζ .

we varied α as 1/15, 1/30, and 1/100 in the model equation. For comparison, we also executed the NSW model.

Figure 5 shows the computed and empirical relations between Q^* and ζ . According to the empirical curve, Q^* increases with increasing ζ (or decreasing L_w/H_0). In contrast, the NSW model predicts a nearly constant Q^* , which is close to a theoretical value for broad-crested weirs. This discrepancy is attributed to the underestimated overflow rate, because the centrifugal effect is absent in this model. When large-depth overflow occurs on a narrow-crested levee, such centrifugal effects cannot be ignored. The relations computed by the modified equation are better matched to the empirical curve. The best agreement is achieved for $\alpha = 1/30$, although $\alpha = 1/100$ also yields similar results. As previously illustrated in Figure 3, excessively small α produces unrealistic oscillations in the upstream water surface, which manifest as increased data scattering in Figure 5. Therefore, we conclude that when simulating levee overflows in the present model, the optimum α value for model accuracy and robustness should lie somewhere around 1/30.

4. Conclusion

In the present study, we demonstrated the importance of non-hydrostatic pressure in simulations of long wave flooding over coastal levees, on which the flow suddenly transits from subcritical to supercritical regime. Neglecting the non-hydrostatic pressure leads to underestimation of the overflow rate, especially at large flow depths and curvatures. Although the model performance can be potentially improved by adding fully nonlinear Boussinesq terms to the model equation, the classical Boussinesq-type equation induces excessive oscillations immediately upstream of the levee crest, which might destabilize the model. The unwanted oscillations can be reduced by a modification term with a free parameter α . The value of α was optimized at around 1/30 through comparisons between the model and existing experimental data. Therefore, the standard model of coastal flood simulation, which is based on the nonlinear shallow water equations, potentially underestimates large-scale flood events on coastal areas fronted by steep landforms, such as dunes and levees.

Acknowledgements

This study was supported by the Special Project "Integrated Research Project on Seismic and Tsunami Hazards around the Sea of Japan" from the Ministry of Education, Culture, Sports, Science, and Technology of Japan.

References

- Bonneton P., Chazel F., Lannes D., Marche F., Tissier M., 2011. A splitting approach for the fully nonlinear and weakly dispersive green-naghdi model. *Journal of Computational Physics*, 230(4): 1479-1498.
- Bouchut F., Mangeney-Castelnau A., Perthame B. and Vilotte J. P., 2003. A new model of Saint Venant and Savage-Hutter type for gravity driven shallow water flows. *Comptes rendus mathématique*, 336(6): 531-536.
- Dressler R. F., 1978. New nonlinear shallow-flow equations with curvature. *Journal of Hydraulic Research*, 16(3): 205-222.
- Dutykh D. and Clamond D., 2011. Shallow water equations for large bathymetry variations. *Journal of Physics A: Mathematical and Theoretical*, 44(33): 332001.
- Fenton J. D., 1996. Channel flow over curved boundaries and a new hydraulic theory. *Proceedings of 10th Congress, Asia and Pacific Division of International Association for Hydraulic Research*, 266-273.
- Fritz H. M. and Hager W. H., 1998. Hydraulics of embankment weirs. *Journal of Hydraulic Engineering*, 124(9): 963-971.
- Goto C., 1984. Equations of nonlinear dispersive long waves for a large Ursell number, *Proceedings of JSCE*; 351/II-2: 193-201.
- Harten A. and Hyman J. M., 1983. Self adjusting grid methods for one-dimensional hyperbolic conservation laws. *Journal of Computational Physics*, 50(2): 235-269.
- Hu K., Mingham C. G. and Causon D. M., 2000. Numerical simulation of wave overtopping of coastal structures using the non-linear shallow water equations. *Coastal Engineering*, 41(4): 433-465.
- Kato, F., Suwa, Y., Watanabe, K. and Hatogai, S., 2012. Mechanisms of coastal dike failure induced by the Great East Japan Earthquake Tsunami. *Proceedings of the 33rd International Conference on Coastal Engineering*, 40.
- Keller J. B., 2003. Shallow-water theory for arbitrary slopes of the bottom. *Journal of Fluid Mechanics*, 489: 345-348.

- Le Roy S., Pedreros R., Andre C., Paris F., Lecacheux S., Marche F. and Vinchon C., 2014. Coastal flooding of urban areas by overtopping: dynamic modelling application to the Johanna storm (2008) in Gavres (France). *Natural Hazards and Earth System Sciences*, 2(8): 4947-4985.
- Lynett P. J., Melby J. A. and Kim D. H., 2010. An application of Boussinesq modeling to hurricane wave overtopping and inundation. *Ocean Engineering*, 37(1): 135-153.
- Madsen P., Murray R. and Sorensen O., 1991. A new form of the Boussinesq equations with improved linear dispersion characteristics. *Coastal Engineering*, 15(4): 371-388.
- Roe P. L., 1981. Approximate riemann solvers, parameter vectors, and difference schemes. *Journal of Computational Physics*, 43(2): 357-372.
- Roe, P. L., 1986. Characteristic-based schemes for the Euler equations. *Annu. Rev. Fluid Mech.*, 18: 337-365.
- Roerber V., Cheung K. F. and Kobayashi M. H., 2010. Shock-capturing Boussinesq-type model for nearshore wave processes. *Coastal Engineering*, 57(4): 407-423.
- Seabra-Santos F. J., Renouard D. P. and Temperville A. M., 1987. Numerical and experimental study of the transformation of a solitary wave over a shelf or isolated obstacle. *Journal of Fluid Mechanics*, 176: 117-134.
- Shimozono T. and Sato S., 2016. Coastal vulnerability analysis during tsunami-induced levee overflow and breaching by a high-resolution flood model. *Coastal Engineering*, 107: 116-126.
- Shimozono T., Tajima Y., Kennedy A. B., Nobuoka H., Sasaki J. and Sato S., 2015, Combined infragravity wave and sea-swell runup over fringing reefs by super typhoon Haiyan. *Journal of Geophysical Research: Oceans*, 120(6): 4463-4486.
- Stelling G. and Duinmeijer S., 2003. A staggered conservative scheme for every Froude number in rapidly varied shallow water flows. *International Journal for Numerical Methods in Fluids*, 43(12): 1329-1354.
- Sweby P. K., 1984. High resolution schemes using flux limiters for hyperbolic conservation laws. *SIAM journal on numerical analysis*, 21(5): 995-1011.
- Tonelli M. and Petti M., 2013. Numerical simulation of wave overtopping at coastal dikes and low-crested structures by means of a shock-capturing Boussinesq model. *Coastal Engineering*, 79: 75-88.
- Tuan T. Q. and Oumeraci H., 2010. A numerical model of wave overtopping on seadikes. *Coastal Engineering*, 57(8): 757-772.
- Wei G. and Kirby J., 1995. Time-dependent numerical code for extended Boussinesq equations. *Journal of Waterway, Port, Coastal and Ocean Engineering*, 121(5): 251-261.
- Yee H. C. 1989. A class of high resolution explicit and implicit shock-capturing methods. *NASA-TM-101088*.
- Yee H. C., Sandham N. D. and Djomehri M. J., 1999. Low-dissipative high-order shock-capturing methods using characteristic-based filters. *Journal of Computational Physics*, 150(1): 199-238.